Int J Mech Mater Des manuscript No.
(will be inserted by the editor)

A material point method model and ballistic limit equation for hyper velocity impact of multi-layer fabric coated aluminum plate

the date of receipt and acceptance should be inserted later

Abstract A multi-layer fabric coated aluminum plate is usually used in the hard upper torso of space suit to protect astronauts from getting hurt by space dust. In this paper, the protective performance of the multi-layer fabric coated aluminum plate is investigated. To establish its ballistic limit equation, thirteen hyper velocity impact tests with different impact velocities (maximum velocity is 6.19km/s) and projectile diameters have been conducted. To provide data for impact velocity higher than 6.2km/s which is hard to be obtained by tests due to the limitations of test equipment capacity, a material point method (MPM) model is established for the multi-layer fabric coated aluminum plate and validated/corrected using the test results. The numerical results obtained using the corrected MPM model for impact velocity higher than 6.2km/s are used together with the test results to develop the ballistic limit equation. The corrected MPM model and the ballistic limit equation developed for the multi-layer fabric coated aluminum plate provide an effective tool for the space suit design.

Keywords Hyper velocity impact · Material point method · Multi-layer fabric coated aluminum plate · Space suit · Ballistic limit equation

1 Introduction

Due to their excellent impact-resistance, anti-fatigue and energy absorption capacity, fabrics and flexible composites are frequently used in protective structures to enhance their protective capacity [9]. For example, the multi-layer fabric coated aluminum plate structure, as shown in Fig.1(a), is used in the hard upper torso (HUT) of space suit to protect astronauts from getting hurt by space dust, where the multi-layer fabric consists of a outer-layer fabric, a multi-layer insulation (MLI) layer and a liner layer, as shown in Fig.1(b). The MLI layer is composed of aluminized films separated by gauzes [32].

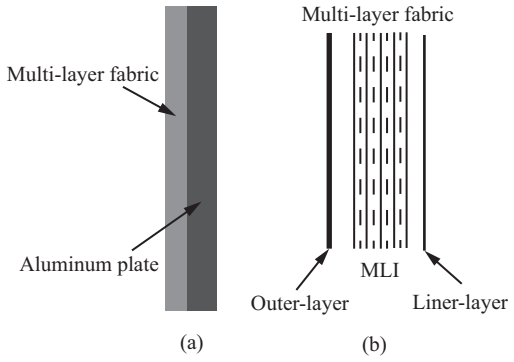

Fig. 1 (a) Multi-layer fabric coated aluminum plate; (b) Multi-layer fabric

The investigation on the protective performance of the multi-layer fabric structures are generally based on the hyper velocity impact test. William et al. [29] studied the protective performance of different fabrics of space suit through hyper velocity impact test. Christiansen et al. [5] investigated the protective performance of different fabrics combined in different forms, and established a ballistic limit equation with different structural forms. They also verified the fact that protective capacity can be increased by using flexible

materials and appropriate structural forms, and evaluated the debris risk [5]. Christiansen et al. [4] described results of impact tests with velocity greater than 10 km/s on Nextel/Kevlar stuffed Whipple and all-aluminum shields. Liu et al. also carried out hyper velocity impact tests of glass, extravehicular space suit and satellite electronic box [24]. However, due to the limitations of test equipment capacity, the limit speed of hyper velocity impact test is generally below 7km/s. With the rapid development of simulation technology, the numerical simulation has become a good supplement for test with strong repeatability.

The hyper velocity impact simulation is a big challenge to numerical methods because it involves extreme localized deformation, fragmentation, melting and vaporization. The Lagrangian approach suffers from the difficulties associated with grid distortion and element entanglement, while the Eulerian approach suffers from the difficulties associated with tracking material interfaces and modeling history-dependent materials. By absorbing the basic idea of both the Lagrangian and Eulerian approaches, the material point method (MPM) [30,31,36] discretize a continuum body into a set of material points (particles) moving through an Eulerian background grid, as shown in Fig.2. All material properties, such as mass, velocity, stress, strain and state variables, are carried by the particles so that it is easy to track material interfaces and to implement history-dependent material constitutive models. The momentum equations are solved on the background grid, so that there is no grid distortion and element entanglement, which makes the MPM robust in modeling various types of extreme loading events [36]. In recent years, much effort has been devoted to developing the MPM for simulating extreme loading events in our group at Tsinghua University. As a result, a 3D explicit and parallel MPM code, MPM3D, has been developed [28,36], which has implemented various MPM/GIMP algorithms, FEM and its different coupling scheme with MPM. The MPM3D has been successfully applied in various extreme loading events, such as hyper velocity impact [35,23,21,7,27,11,25], penetration [12,15,20,17,18,3], blast [16,26], fluid-structure interactions [19,33].

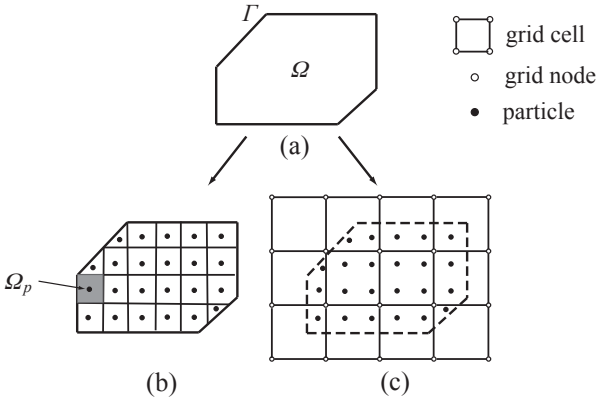

Fig. 2 MPM discretization [36]

This paper investigates the protective performance of a multi-layer fabric coated aluminum plate. To establish its ballistic limit equation, we have conducted thirteen hyper velocity impact tests with different impact velocities and projectile diameters. However, due to the limitations of the experiment equipment capacity, the impact velocity in the tests are less than 6.2km/s. To provide data for higher impact velocity, numerical simulations are carried out using the MPM model with MPM3D. To provide reliable numerical results, the MPM model used must be validated and corrected using the test results. The ballistic limit equation is eventually developed based on the test results together with the numerical results.

This paper is organized as follow. Section 2 describes the hyper velocity tests and presents the test results. Section 3 establishes an equivalent laminated plate model of the MLI layer to avoid discretizing each single-layer of the MLI which is too thin. Section 4 summarizes the material models and corresponding material constants used for the multi-layer fabric coated aluminum plate. A MPM model is established in Section 5 for the hyper velocity impact of the multi-layer fabric coated aluminum plate and validated using the test results presented in Section 2. A corrected MPM model is proposed based on the comparison of numerical results and test results, and is used to establish the ballistic limit equation together with the tests in Section 6. Concluding remarks are given in Section 7.

2 hyper velocity impact tests

The ballistic limit equation is used to determine the critical projectile diameter causing perforation on the target, which is an essential tool for determining the minimum shielding requirements for spacecraft. When the projectile diameter is greater than the critical diameter, the projectile will penetrate the specimens.

To obtain the ballistic limit equation for the multi-layer fabric coated aluminum plate and to validate the MPM model established in this paper, the hyper velocity impact tests have been carried out in the

China Aerodynamics Research and Development Center using a 7.6mm-caliber two-stage light gas gun. The velocity is measured by the laser beam shielding method. The pressure inside the target chamber during test is 50Pa, and the sequence laser shadow camera system is used to take pictures for collision process.

The specimens are 200mm × 200mm squares. The outer-layer fabric, MLI layer and liner layer are sewn together along all edges, as shown in Fig. 3(a). The sewn multi-layer fabric is spread on the aluminum plate, and then punched with a metallic frame with an 140mm × 140mm square opening in the center at four sides. The whole test piece is fixed on a bracket inside the target chamber through bolted connection, as shown in Fig.3(b).

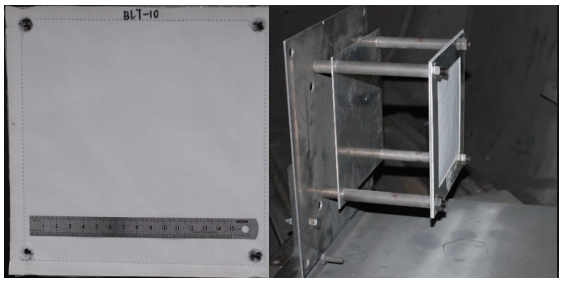

(a) (b)

Fig. 3 (a) The sewn multi-layer fabric; (b) The test piece fixed on the bracket

The critical diameter is difficult to be obtained directly from the test. Therefore, we try to obtain the minimum projectile diameter penetrating the specimen and the maximum projectile diameter without penetrating the specimen at the same speed as much as possible in the test. Thus, thirteen tests were conducted with different project diameter d_{p} and impact speed V, as listed in Table 1. The diameter of the projectile is from 0.8mm to 1.4mm, while the measured impact speed is from 2.93km/s to 6.19km/s. The impact angle is 0 degree.

Table 1 The test parameters and results

Test cases	d_{p} (mm)	V (km/s)	Penetrated (Y/N)
01	1.0	3.09	N
02	1.2	2.93	N
03	1.4	3.02	Y
04	1.0	3.98	Y
05	1.2	4.03	Y
06	0.9	3.85	N
07	1.0	4.30	Y
08	0.8	4.47	N
09	0.8	4.91	N
10	1.2	4.99	Y
11	1.0	5.15	Y
12	0.9	6.11	N
13	1.0	6.19	Y

The test results are listed in the rightmost column of Table 1, which indicate whether the aluminum plate is penetrated. These results are also plotted in Fig.20, which shows that the critical penetration diameter is monotonically decreasing when the impact velocity is smaller than 4.5km/s. Within this velocity range, the impact only lead to deformation of the projectile. The damage form of the test specimen is a single crater or a single shearing aperture, as shown in Fig.4. When the impact velocity is greater than 4.5km/s, the critical penetration diameter will increase with the increase of impact velocity. Within this velocity range, the damage form of the test specimen illustrates that the projectile has been already broken after it penetrates the layers of fabric so that these broken pieces lead to many circular pits on the aluminum plate, as shown in Fig.5.

More test results will be provided in Section 5 to validate our numerical model.

3 Equivalent laminated plate model of the MLI layer

As shown in Fig.1, the multi-layer fabric coated aluminum plate consists of a outer-layer fabric, a MLI layer, a liner layer and a aluminum plate. A MLI layer consists of aluminized films separated by gauzes, as shown in Fig.6. As a meshfree method, the MPM is capable of modeling material and structure with complex internal structure, such as aluminum foam and honeycomb sandwich [21,22,23]. However, discretizing

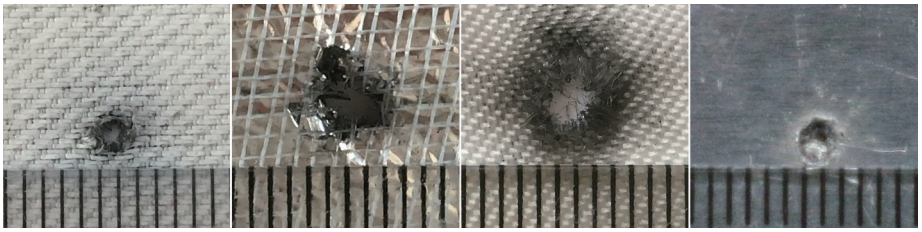

Fig. 4 The damage configuration of the test case 01: $d_{\mathrm{p}} = 1.0\mathrm{mm}$, $V = 3.09\mathrm{km/s}$

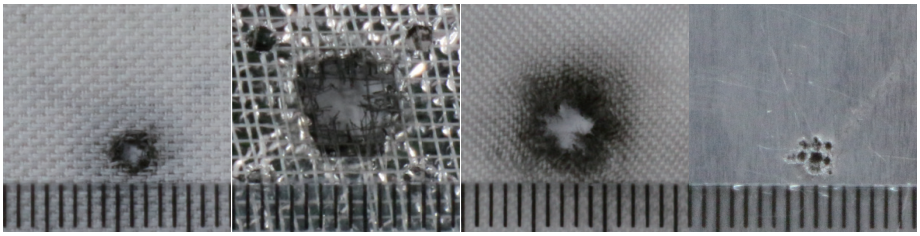

Fig. 5 The damage configuration of the test case 09: $d_{\mathrm{p}} = 0.8\mathrm{mm}$, $V = 4.91\mathrm{km/s}$

each aluminized film and gauze in a MLI layer into particles will result in too may particles which is cost prohibitive, because each single-layer of the MLI layer is too thin (the minimum thickness is about 18μm). Therefore, the MLI layer has to be idealized as a single-layer material with equivalent material properties properly determined.

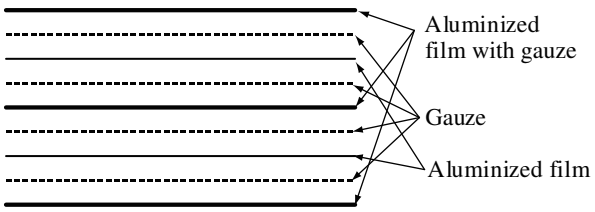

Fig. 6 A MLI layer

3.1 Laminated plate model

Fig.6 illustrates the schematic diagram of the MLI layer used in this paper, which is made up of 9 layers symmetrical with respect to the central axis. The MLI layer can be idealized as a symmetric laminated plate model (as shown in Fig.7), with each single-layer simplified as a transversely isotropic material on the x-y plane where the length and width are located. Due to the flexibility, these materials which constitute the laminated plate can not bear bending and twisting. Therefore, the bending rigidity and coupling rigidity of the laminates are ignored, and only the tensile rigidity is taken into account.

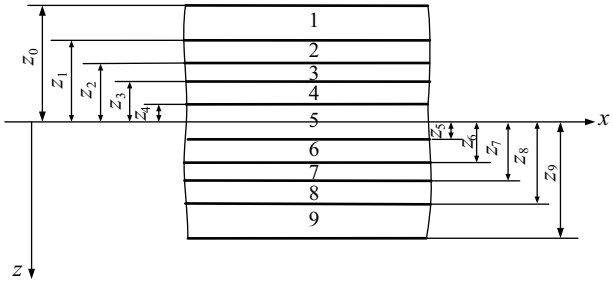

Fig. 7 z coordinates of each layer of the MLI

Let the laminated plate be subjected to the axial tensile load N_x, and the loads in other directions are 0. Thus, the load-strain relationship of the laminated plate can be stated as

$$\begin{bmatrix} N_x \\ 0 \\ 0 \end{bmatrix} = \boldsymbol{A} \begin{bmatrix} \varepsilon_x \\ \varepsilon_y \\ \gamma_{xy} \end{bmatrix} \tag{1}$$

where ε_x, ε_y and γ_{xy} are the strain components of the laminated plate, $\boldsymbol{A}$ is the equivalent tensile rigidity of the laminated plate defined by

$$\boldsymbol{A} = \sum_{k=1}^{n} t_k b \boldsymbol{Q}_k \tag{2}$$

where b is the width of the plate, $t_k = z_k - z_{k-1}$ is the thickness of the kth layer, and

$$\boldsymbol{Q}_k = \begin{bmatrix} \dfrac{E_k}{1-\nu_k^2} & \dfrac{\nu_k E_k}{1-\nu_k^2} & 0 \\ \dfrac{\nu_k E_k}{1-\nu_k^2} & \dfrac{E_k}{1-\nu_k^2} & 0 \\ 0 & 0 & \dfrac{E_k}{2\left(1+\nu_k\right)} \end{bmatrix} \tag{3}$$

with E_k and ν_k denoting the Young's modulus and Poisson's ratio of the kth layer, respectively.

Let the laminated plate is equivalent to a single-layer plate with the same thickness $t = \sum_{k=1}^{n} t_k$. Supposing the equivalent elastic modulus and Poisson's ratio of the single-layer plate are E and ν, respectively, we have

$$\boldsymbol{A} = tb \begin{bmatrix} \dfrac{E}{1-\nu^2} & \dfrac{\nu E}{1-\nu^2} & 0 \\ \dfrac{\nu E}{1-\nu^2} & \dfrac{E}{1-\nu^2} & 0 \\ 0 & 0 & \dfrac{E}{2\left(1+\nu\right)} \end{bmatrix} \tag{4}$$

The equivalent Young's modulus and Poisson's ratio of the single-layer plate E and ν can be calculated by substituting Eq.(2) into Eq.(4).

The limit load of the laminated plate can be determined through strength analysis. Let N_x gradually increases from zero until all layers of material are yield or failed. The stress of each single-layer material is calculated and then the Von Mises yield criterion and the maximum principal strain failure criterion are used to determine which layer will be yielded or failed first. When a single-layer of the laminated plate is yielded or failed, its rigidity will be weakened so that the slope in the load-displacement curve of the laminate will be decreased. With the increase of external load, the numbers of failed layers are increased and the rigidity will be lower and lower until it becomes zero. Thus, the laminated plate can no longer bear the load and the external load at this moment is the limit load of the laminated plate. The basic steps of calculation are summarized as follows:

1) The stress-strain relationship of the kth layer laminate is

$$\begin{bmatrix} \sigma_{xk} \\ \sigma_{yk} \\ \tau_{xyk} \end{bmatrix} = \boldsymbol{Q}_k \begin{bmatrix} \varepsilon_{xk} \\ \varepsilon_{yk} \\ \gamma_{xyk} \end{bmatrix} = \boldsymbol{Q}_k \boldsymbol{A}^{-1} \begin{bmatrix} N_x \\ 0 \\ 0 \end{bmatrix} \tag{5}$$

where the second equality is due to the fact that the strain of each single-layer is the same as that of the laminated plate.

2) The Von Mises yield criterion $\sigma_{xk}^2 + \sigma_{yk}^2 + \left(\sigma_{xk} - \sigma_{yk}\right)^2 = 2\sigma_{\mathrm{y}k}^2$ and the maximum principal strain failure criterion $\varepsilon_1 > \varepsilon_{\mathrm{f}k}$ are used to solve the corresponding N_x when yield or failure of various layers occurs, where $\sigma_{\mathrm{y}k}$ and $\varepsilon_{\mathrm{f}k}$ are the yield strength and failure strain of the kth layer, respectively, ε_1 is the maximum principal strain of the laminate.

3) Update $\boldsymbol{Q}_k$ and $\boldsymbol{A}$. If yield happens in the kth layer, its rigidity coefficient $\boldsymbol{Q}_k$ is weakened to

$$\widetilde{\boldsymbol{Q}}_k = \frac{E_{\mathrm{t}k}}{E_k} \boldsymbol{Q}_k \tag{6}$$

where $E_{\mathrm{t}k}$ is the tangent modulus of the kth layer. If failure happens in the kth layer, its weakened rigidity coefficient should be $\widetilde{\boldsymbol{Q}}_k = 0$. If the kth layer is neither failed nor yield, its rigidity coefficient shall remain unchanged, i.e. $\widetilde{\boldsymbol{Q}}_k = \boldsymbol{Q}_k$.

Thus, the weakened rigidity of the laminated plate can be obtained as

$$\widetilde{\boldsymbol{A}} = \sum_{k=1}^{n} \widetilde{\boldsymbol{Q}}_k t_k b \tag{7}$$

4) Update the stress of each layer. The stress increment of kth layer is

$$\begin{bmatrix} \Delta\sigma_x \\ \Delta\sigma_y \\ 0 \end{bmatrix}_k = \widetilde{\boldsymbol{Q}}_k \begin{bmatrix} \Delta\varepsilon_x \\ \Delta\varepsilon_y \\ 0 \end{bmatrix}_k = \widetilde{\boldsymbol{Q}}_k \widetilde{\boldsymbol{A}}^{-1} \begin{bmatrix} \Delta N_x \\ 0 \\ 0 \end{bmatrix} \tag{8}$$

5) Continue to increase the axial tension N_x, and repeat steps 1) to 4) until all layers fail.

The stress-strain curve of the laminated plate can be obtained though above calculation. The kinks in the curve correspond to the yield points and failure points of the different layers of the laminated plate.

3.2 Determination of material properties of each layer

The material parameters of each layer can be obtained by carrying out various mechanical tests. The elastic properties of the single-layer material can be obtained by static tests, while the material behavior at high strain rates needs to be obtained under dynamic test conditions[37]. Because each single-layer of the MLI is very soft and slim, typical tests under dynamic loading conditions such as Hopkinson test and shear test are very difficult to conduct, if not impossible. Therefore, the material parameters of each single layer is obtained in this paper by the quasi-static axial tensile test.

The quasi-static axial tensile tests are carried out on the Zwick/Roell tensile testing machine with upper-beam moving at speed of 5mm/min. The test pieces are made into long strips with a width of 20mm and a length of 100mm. The specimen breaking is taken as the terminate condition.

The stress-strain curves obtained by the axial tensile tests are shown as Fig.8. Based on these stress-strain curves, the elastic modulus E, yield stress σ_{y}, tangent modulus E_{t} and failure strain ε_{f} of each single-layer can be calculated, as listed in Table 2. The Poisson's ratio is determined by FEM simulation using LS-DYNA to match the numerical results with the axial tensile test data.

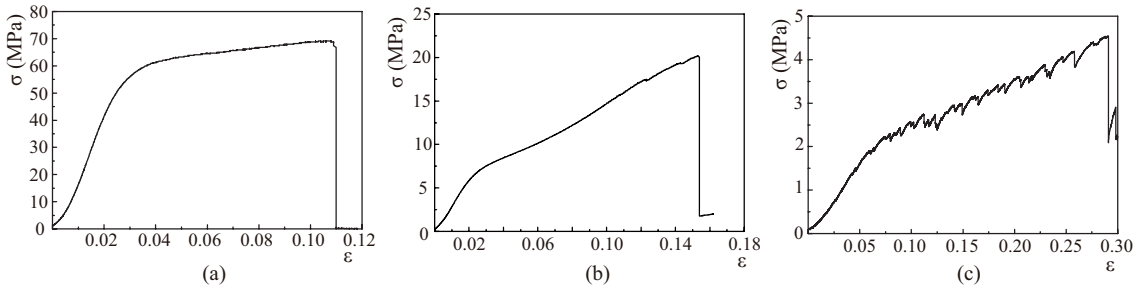

Fig. 8 Stress-strain curves of (a) Aluminized film, (b) Aluminized film with gauze and (c) Gauze

Table 2 The material parameters of the single-layers of the MLI

	E(MPa)	σ_{y}(MPa)	E_{t}(MPa)	ε_{f}	ν
Aluminized film	2478.9	58	114	0.11	0.2
Aluminized film with gauze	294	6.5	109	0.15	0.2
Gauze	33.17	2.0	11.7	0.28	0.1

3.3 Validation of the laminated plate model

In order to validate the equivalent laminated plate model of the MLI layer established in Section 3.1, the tensile test of the MLI is carried out. The stress-strain curve obtained by the test is compared with that obtained by the laminate model in Fig.9. There are three yield stress points denoted by a, b and c in Fig.9 at which a single-layer is yielded. Fig.9 shows that the results calculated by the laminated plate model agree well with the test results in the elastic and plastic regions, but shows significant discrepancy after the first ply failure point d. The main reason for the discrepancy is that the layers of the test pieces is hand-paved, so that some layers are tight while some layers are relatively loose.

The elastic modulus E, Poisson's ratio ν, yield stresses σ_{y1}, σ_{y2} and σ_{y3}, limit stress σ_{limit}, and tangent modulus E_{t} of the equivalent laminated plate can be calculated using the theory presented in Section 3.1. Take the first yield stress σ_{y1} as the yield stress of the equivalent laminated plate. There are three segments ab, bc and cd in the curve from the first yield stress points a to the first ply failure point d. The slope of these segments represents the tangent modulus of the laminated plate. The first segment ab can be

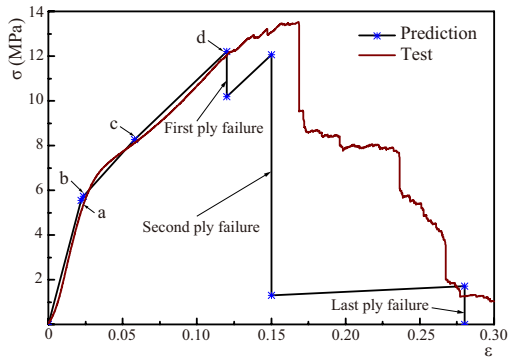

Fig. 9 Stress-strain curves of the MLI layer obtained by the test and the laminated plate model prediction

neglected because its length is very short. The slopes of bc and cd are very close, so that these two lines can be approximated as a straight line bd, whose slope is taken as the tangent modulus of the laminated plate. The material constants determined for the MLI are list in Table 4.

4 Material models

The projectile and aluminum plate are made of 2A12 aluminum alloy and 5A06 aluminum alloy, respectively. The Johnson-Cook model is used with the Gruneisen equation of state to model the mechanical behavior of these alloys. The Johnson-Cook model [13] [14] is mainly used to describe material behavior of metal materials subject to large strain, high temperature and high strain rate, whose yield stress is given by

$$\sigma_{\mathrm{y}} = \left(A + B\varepsilon^{\mathrm{p}n}\right)\left(1 + C\ln\dot{\varepsilon^{*}}\right)\left(1 - T^{*m}\right) \tag{9}$$

where $\dot{\varepsilon}^{*} = \dot{\varepsilon}^{\mathrm{p}}/\dot{\varepsilon}_0$ is the dimensionless equivalent plastic strain rate, $\dot{\varepsilon}_0 = 1\mathrm{s}^{-1}$ is the effective plastic strain rate of the quasi-static test used to determine the yield and hardening parameters, $\dot{\varepsilon}^{\mathrm{p}} = \triangle\varepsilon^{\mathrm{p}}/\triangle t$ is the plastic strain rate, A, B, C, m and n are the material constants, $T^{*} = (T - T_{\mathrm{r}})(T_{\mathrm{m}} - T_{\mathrm{r}})$ is the dimensionless temperature, T_{r} and T_{m} are the room temperature and melt temperature, respectively.

The Mie-Gruneisen equation of state (EOS) is mainly used to describe the thermo-mechanical behavior of metallic solids, which is stated as

$$p = p_{\mathrm{H}}\left(1 - \frac{\mu\gamma}{2}\right) + \gamma_0 E \tag{10}$$

where p_{H} is the pressure on the Hugoniot, $\mu = \rho/\rho_0 - 1$ is the coefficient of compressibility, $\gamma = \gamma_0\rho_0/\rho$ is the Gruneisen coefficient, E_0 is the internal energy per unit reference volume, c_0 is the sound speed of the material, γ_0 and s are the material constants.

The maximum tension stress failure criteria, $\sigma_1 > \sigma_{\max}$, is used to simulate peel-off of the aluminum plate and cratering failure, where σ_1 is the maximum principal stress, $\sigma_{\max}$ is the material constant.

The material constants of 2A12 aluminum alloy and 5A06 aluminum alloy are taken from the literature [6,8], and summarized in Table 3.

Table 3 Material constants of the projectile and aluminum plate

Parameter	2A12 aluminum alloy	5A06 aluminum alloy
$\rho\,(\mathrm{g/mm^3})$	2.77×10^{-3}	2.67×10^{-3}
E(MPa)	7.17×10^{4}	7.182×10^{4}
A(MPa)	265	207
ν	0.33	0.33
B(MPa)	426	426
C	0.015	0.015
n	0.34	0.34
m	1.0	1.0
C_{p}(J/kg K)	904	853
T_{m}(K)	900	864
$\sigma_{\max}$(MPa)	2500	2200
c_0(m/s)	5328	5328
s	1.11	1.338
γ_0	2.0	2.0

Both the outer-layer fabric and the MLI layer are modeled by using the elastic-plastic model with the Gruneisen EOS and the maximum principal strain failure model. The elastic-plastic material constants and failure strain of the MLI layer have been obtained in Section 3, while the Gruneisen EOS constants are

taken from the literature[10]. The elastic-plastic material constants and failure strain of the outer-layer are obtained by quasi-static axial tensile tests, while the Gruneisen EOS constants are taken from the literature[2]. These constants are listed in Table 4.

The stress-strain curve obtained by quasi-static axial tensile test shows that the liner layer behaviors elastically. Thus, the liner layer is modeled by the elastic model with the Gruneisen EOS and the maximum principal strain failure mode. The elastic material constants and failure strain are obtained from the tensile test, while the Gruneisen EOS constants are taken from the literature[34,1], see Table 4.

Table 4 Material constants of the multi-layer fabric

Parameter	Outer-layer fabric[2]	MLI layer[10]	Liner layer[34,1]
$\rho\,(\mathrm{g/mm^3})$	0.96×10^{-3}	0.267×10^{-3}	0.65×10^{-3}
E(MPa)	1905	261.27	248.59
ν	0.43	0.195	0.3
σ_{y} (MPa)	188	5.54	
E_{t}(MPa)	88.44	66.73	
ε_{f}	0.25	0.11	0.23
c_0(m/s)	5350	2000	1506
s	1.0	1.4	1.32
γ_0	0.766	1.53	0.784

5 Numerical simulation

In the hyper velocity impact test presented in Section 2, the specimen is a 200mm × 200mm × 3mm multi-layer fabric coated aluminum plate. The thicknesses of the outer-layer, MLI layer, liner-layer and aluminum plate are 0.4mm, 1.0mm, 0.2mm and 1.4mm, respectively. In the tests, the minimum impact velocity of the projectile is about 3km/s, and the coated aluminum plate is penetrated in less than 4μs. Since the sound speed of the aluminum plate is 5328m/s, the impact wave travels less than 21.5mm in the aluminum plate during this period. Therefore, to reduce the computational cost, the size of the multi-layer fabric coated aluminum plate is chosen as 28mm × 28mm × 3mm in our numerical studies. The MLI layer is simplified by the equivalent laminated plate model established in Section 3.

5.1 MPM model

Due to symmetry, only one half of the plate is modeled by MPM particles, as shown in Fig.10. There are five parts in the model, namely, the spherical projectile, the outer-layer fabric, the MLI layer, the liner layer and the aluminum plate. The particle spacing is 0.1mm, while the cell size of the background grid is 0.2mm. The symmetric boundary condition is imposed on the symmetry plane, whereas the free boundary condition is imposed on the top and bottom boundaries. The transmitting boundary condition is imposed on the three remaining boundaries to suppress the reflection wave on these artificial boundaries.

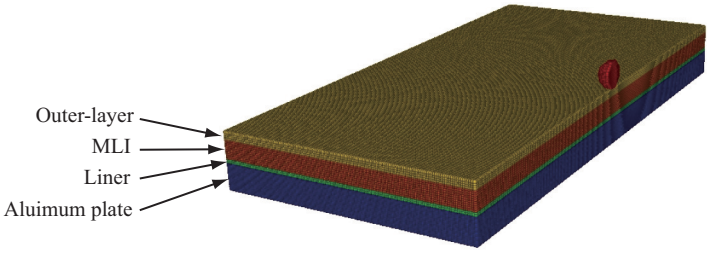

Fig. 10 MPM model of the multi-layer fabric coated aluminum plate

5.2 Numerical simulation of test cases 03 and 05

In order to validate the MPM model, the test cases 03 and 05 listed in Table 1 are simulated using our MPM3D code[28,36] with the MPM model. The final configuration of the outer-layer and aluminum plate obtained by the MPM simulation are compared with the test results in Fig.11 - Fig.14, while the sizes of the perforated holes in horizontal and vertical direction ($D_{\mathrm{h}} \times D_{\mathrm{v}}$) are listed in Table 5.

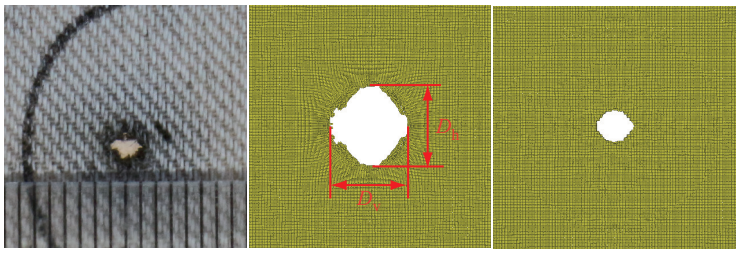

(a) (b) (c)

Fig. 11 The final configuration of the outer-layer for test case 03 obtained by (a) the test, (b) the original MPM model and (c) the corrected MPM model.

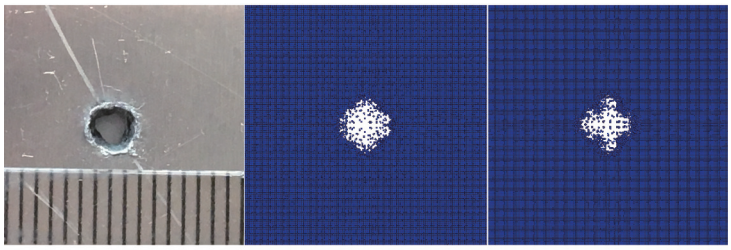

(a) (b) (c)

Fig. 12 The final configuration of the aluminum plate for test case 03 obtained by (a) the test, (b) the original MPM model and (c) the corrected MPM model.

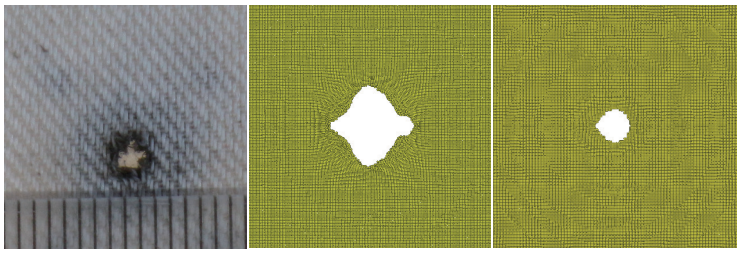

(a) (b) (c)

Fig. 13 The final configuration of the outer-layer for test case 05 obtained by (a) the test, (b) the original MPM model and (c) the corrected MPM model.

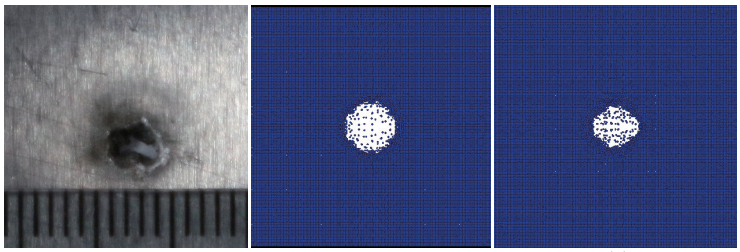

(a) (b) (c)

Fig. 14 The final configuration of the aluminum plate for test case 05 obtained by (a) the test, (b) the original MPM model and (c) the corrected model.

Table 5 Sizes of the perforated holes ($D_h \times D_v$)

	Test case 03 (mm)		Test case 05 (mm)	
	Outer-layer	Aluminum plate	Outer-layer	Aluminum plate
Test	2×1.8	2.2×2	1.8×1.8	2.4×1.1
Original MPM model	5×5	3.5×3.6	5.3×5.2	3.2×3.2
Corrected MPM model	2.7×2.4	3.0×3.4	2.3×2.2	2.9×2.4

Fig.11 - Fig.14 show that the sizes of the perforated hols obtained by the MPM simulation are larger than those of the test, especially the numerical diameters of the holes perforated in the outer-layer are more than 2 times of the test results. One possible reason is that the material constants of the outer-layer are obtained from quasi-static test, rather than from high strain rate test, as discussed in Section 3.2. However, it is difficult to eliminate this error. Another reason is that the MPM model does not agree well with the test specimen. Fig.15 shows a snapshot of the test, which illustrates that the thickness in the middle of the test specimen is obviously larger than that in the fixed end. That is to say, there exists space between the layers, which has not been taken into account in the original MPM model. Thus, the original MPM model should be corrected to include these spaces.

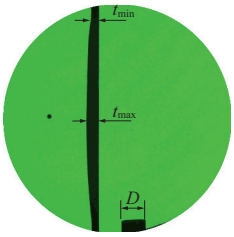

Fig. 15 A snapshot of the test

5.3 Model Correction

Taking the space between layers into account, the original MPM model shown in Fig.10 can be corrected as shown in Fig.16. The outer-layer, MLI layer and liner layer are assumed to be spaced equally, namely $s_1 = s_2$, where s_1 and s_2 denote the space between the adjacent layers. The maximum and minimum thicknesses of the test specimen shown in Fig.15 are measured as $t_{\max} = 8$mm and $t_{\min} = 5$mm. Taking the averaged thickness $t_a = 6.5$mm as the thickness of the test specimen, the total space $s = s_1 + s_2$ can be obtained as the difference between the t_a and the thickness $t = 3.0$mm in the original model. Thus, the spaces can be obtained as $s_1 = s_2 = (t_a - t)/2 = 1.75$mm.

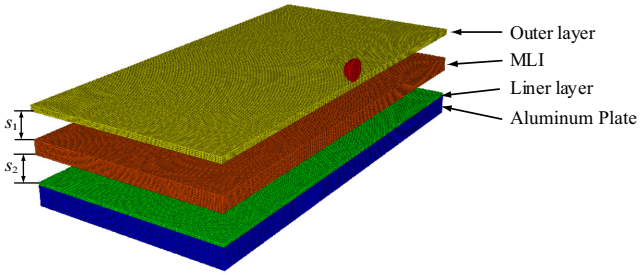

Fig. 16 The corrected MPM model

The hyper velocity impact tests of test cases 03 and 05 are simulated again using the corrected MPM model shown in Fig.16. The final configurations of the outer-layer and the aluminum plate are compared with the test results in Fig.11 - Fig.14, while the sizes of the perforated holes are compared with the test results in Table 5. These comparisons show that the numerical results obtained with the corrected MPM model agree reasonably with the test results.

5.4 Investigation on the out layer damage and debris cloud

Although the corrected MPM model is obtained base on the results of test cases 03 an 05, it should be able to simulate other hyper velocity impact tests with different impact velocity and projectile diameter. For example, the hyper velocity impact of a projectile with a diameter of 3mm at an impact velocity of 4.26km/s is simulated using MPM3D with the corrected MPM model. Fig.17 compares the debris clouds at different times obtained by the MPM simulation with test results. The MPM simulation results clearly shows that when the projectile pierces through the target, the projectile is broken into debris. Most of the debris continues to move forward, while some of them ejects backward, and some of them splashes between the layers. The debris cloud continues to stretch and expand during the process of moving forward and

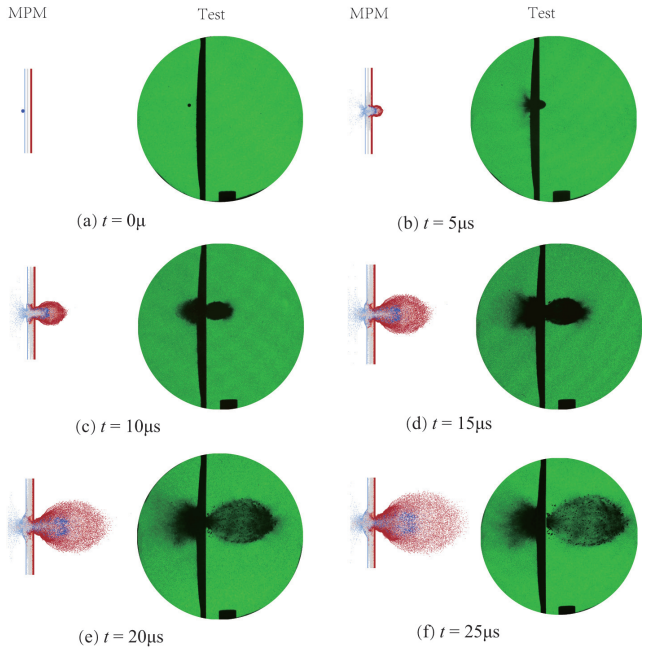

Fig. 17 The debris cloud at different times

forms into an oval bubble. The shape and size of the debris cloud obtained by the MPM simulation agrees well with the test results.

Fig.18 illustrate the configuration of the outer-layer fabric with color representing the von Mises stress at different times. The figures in the font view show that the backwash debris splash between the layers and impact on the outer-layer fabric in the opposite direction, which cause damage to the outer-layer fabric, as shown in the figures in the bottom view. Fig.19 compares the final configuration of the outer-layer fabric obtained by the MPM simulation with the test results. In addition to the perforated hole centered at the impact point, there exist several small holes distributed along a circle centered at the impact point. The diameters of the center hole and the circle obtained by the MPM simulation agree very well with the test results.

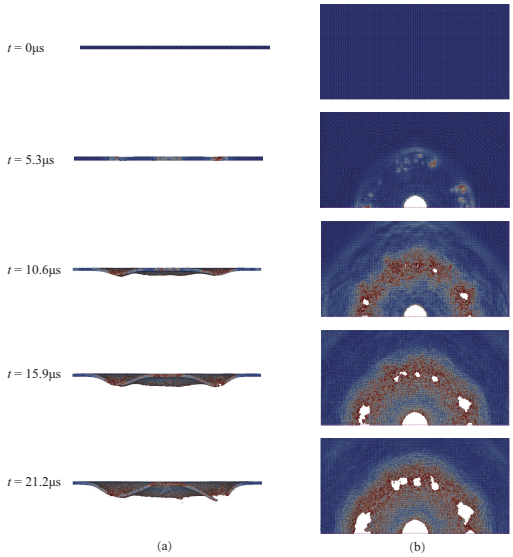

Fig. 18 Configurations of the outer-layer fabric with color representing the stress at different times. (a) the front view; (b) the bottom view.

6 Ballistic limit equation

Christiansen et al.[5] showed that there exist inflection points in the ballistic limit curves of the soft good components of the extravehicular mobility unit (EMU) space suit. Therefore, the ballistic limit equation is

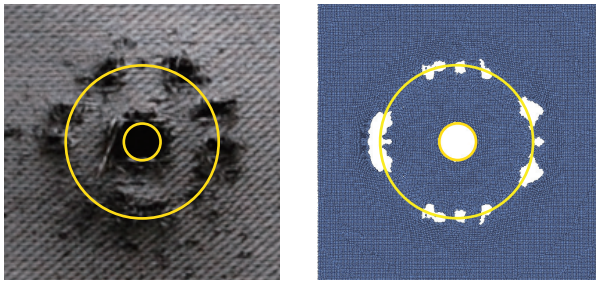

(a) (b)

Fig. 19 Final configuration of the outer-layer obtained by (a) experiment and (b) MPM simulation.

a multi-segment function as[5]

$$d_{\mathrm{c}}=\begin{cases}\frac{C_{\mathrm{L}}}{\rho^{0.5}V^{2/3}\cos\theta^{X}} & V\le V_1\\ \frac{C_{\mathrm{hi}}}{\rho^{0.5}\cos\theta^{0.15}}\frac{(V-V_1)}{(V_2-V_1)}+\frac{C_{\mathrm{li}}}{\rho^{0.5}\cos\theta^{-(0.088-X)}}\frac{(V_2-V)}{(V_2-V_1)} & V_1\le V\le V_2\\ \frac{C_{\mathrm{H}}}{\rho^{0.5}V^{2/3}\cos\theta^{0.45}} & V\ge V_2\end{cases}\tag{11}$$

where θ denotes the impact angle, V is the impact velocity, $V_1=5.1/\cos\theta^{0.132}$, $V_2=6.95/\cos\theta^{0.45}$, C_{H}, C_{L}, C_{hi}, C_{li} and X are coefficients.

Due to the similarity of the multi-layer fabric coated aluminum plate to the EMU soft good components, we employ Eq.(11) as the ballistic limit equation in form for the multi-layer fabric coated aluminum plate, but with different coefficients. Because d_{c} is continuous across $V=V_1$ and $V=V_2$, the coefficients C_{H}, C_{L}, C_{hi} and C_{li} must satisfy the relationships $C_{\mathrm{hi}}=(6.95)^{-2/3}C_{\mathrm{H}}$ and $C_{\mathrm{li}}=(5.1)^{-2/3}C_{\mathrm{L}}$. Thus, the coefficients C_{hi} and C_{li} can be eliminated from Eq.(11).

By carefully examining Eq.(11), we propose a generalized ballistic limit equation as

$$d_{\mathrm{c}}=\begin{cases}\frac{C_{\mathrm{L}}}{\rho^{0.5}V^{2/3}\cos\theta^{X}} & V\le V_1\\ \frac{C_{\mathrm{H}}}{\rho^{0.5}V_{\mathrm{H}}^{2/3}\cos\theta^{-(\frac{2}{3}S_{\mathrm{H}}-X_{\mathrm{H}})}}\frac{(V-V_1)}{(V_2-V_1)}+\frac{C_{\mathrm{L}}}{\rho^{0.5}V_{\mathrm{L}}^{2/3}\cos\theta^{-(\frac{2}{3}S_{\mathrm{L}}-X)}}\frac{(V_2-V)}{(V_2-V_1)} & V_1\le V\le V_2\\ \frac{C_{\mathrm{H}}}{\rho^{0.5}V^{2/3}\cos\theta^{X_{\mathrm{H}}}} & V\ge V_2\end{cases}\tag{12}$$

where $V_1=V_{\mathrm{L}}/\cos\theta^{S_{\mathrm{L}}}$, $V_2=V_{\mathrm{H}}/\cos\theta^{S_{\mathrm{H}}}$. The ballistic limit equation (11) is a special case of the generalize equation (12) with $S_{\mathrm{H}}=0.45$, $S_{\mathrm{L}}=0.132$, $X_{\mathrm{H}}=0.45$, $V_{\mathrm{H}}=6.95$ and $V_{\mathrm{L}}=5.1$.

Taking Eq.(12) as the ballistic limit equation for the multi-layer fabric coated aluminum plate, we need to determine the eight coefficients (V_{L}, V_{H}, C_{L}, C_{H}, S_{L}, S_{H}, X and X_{H}) based on the test data or/and numerical results. It can be shown that the critical diameter d_{c} is only related to V_{L}, V_{H}, C_{L} and C_{H} if the impact angle $\theta=0$ï¿œ, namely

$$d_{\mathrm{c}}=d_{\mathrm{c}}\left(V,V_{\mathrm{L}},V_{\mathrm{H}},C_{\mathrm{L}},C_{\mathrm{H}}\right)\tag{13}$$

We have conducted 13 tests with impact angle $\theta=0$ï¿œ for impact velocity $V<6.2$km/s, but not for impact velocity $V>6.2$km/s due to the limitations of the test equipment capacity. Therefore, we conducted numerical tests using the corrected MPM model for impact velocity of 7km/s, 8km/s and 9km/s. For each specified impact velocity, many cases have been tried with different projectile diameters to obtain the minimum projectile diameter d_{Ymin} that penetrates the target and the maximum projectile diameter d_{Nmax} that does not penetrate the target, as listed in Table 6.

Table 6 Numerical simulation cases for impact angle $\theta=0°$

V(km/s)	d_{Ymin}(mm)	d_{Nmax}(mm)
2	1.42	1.38
3	1.22	1.18
4	1.12	1.08
5	0.98	0.94
6	0.84	0.80
7	0.92	0.88
8	0.86	0.82
9	0.84	0.80

The numerical results for impact velocity of 7km/s, 8km/s and 9km/s together with the test results listed in Table 1 are used to fit the ballistic limit equation (13). The coefficients are obtained as $V_{\mathrm{L}}=4.73$km/s,

$V_{\mathrm{H}} = 6.56\mathrm{km/s}$, $C_{\mathrm{L}} = 13\mathrm{kg}^{1/2}\mathrm{s}^{-2/3}\mathrm{m}^{1/6}$ and $C_{\mathrm{H}} = 18\mathrm{kg}^{1/2}\mathrm{s}^{-2/3}\mathrm{m}^{1/6}$ by minimizing the mean square fitting error

$$e(V_{\mathrm{L}}, V_{\mathrm{H}}, C_{\mathrm{L}}, C_{\mathrm{H}}) = \frac{1}{N}\sum_{k=1}^{N}(d_{\mathrm{c}}(V_k, V_{\mathrm{L}}, V_{\mathrm{H}}, C_{\mathrm{L}}, C_{\mathrm{H}}) - \hat{d}_{ck})^2 \tag{14}$$

where $N = 19$ is the total number of points used to fit the equation, $d_{\mathrm{c}}\left(V_k, V_{\mathrm{L}}, V_{\mathrm{H}}, C_{\mathrm{L}}, C_{\mathrm{H}}\right)$ is the fitted value, $\hat{d}_{ck}$ is the test value and numerical value. The fitted ballistic limit curve for impact angle $\theta = 0$ï¿œ is plotted in Fig.20.

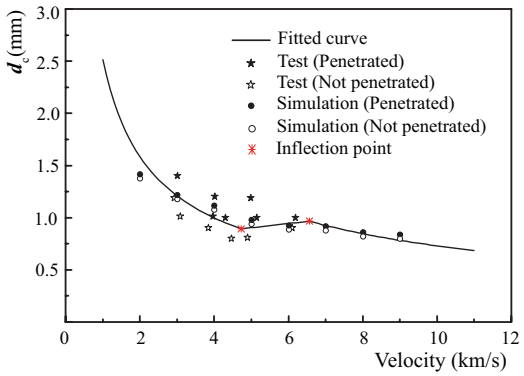

Fig. 20 Fitted ballistic limit curve for impact angle $\theta = 0°$

To further validate our corrected MPM model, the simulation results obtained for the impact velocity $V \leq 6\mathrm{km/s}$ are also plotted in Fig.20. It shows that the critical diameter obtained by our corrected MPM model for impact velocity $V \leq 6\mathrm{km}$ agrees very well to the fitted curve obtained from the test results for impact velocity $V < 6.2\mathrm{km/s}$ and the numerical results for impact velocity $V \geq 7\mathrm{km/s}$. This further verifies that our corrected MPM model is able to well predict the hyper velocity impact behavior of the multi-layer fabric coated aluminum plate.

To further determine the remaining coefficients, we conducted many numerical tests for impact angle $\theta = 45°$ and $\theta = 60°$ with different impact velocities. For each specific impact velocity, many cases have been tried out with different projectile diameters to obtain the minimum and maximum projectile diameters, as listed in Table 7.

Table 7 Numerical simulation cases for impact angle $\theta = 45°$ and $\theta = 60°$

	45°		60°	
$V(\mathrm{km/s})$	$d_{\mathrm{Ymin}}(\mathrm{mm})$	$d_{\mathrm{Nmax}}(\mathrm{mm})$	$d_{\mathrm{Ymin}}(\mathrm{mm})$	$d_{\mathrm{Nmax}}(\mathrm{mm})$
2	1.72	1.68	2.17	2.13
3	1.32	1.28	1.82	1.78
4	1.07	1.03	1.62	1.58
4.5	1.01	0.97	1.32	1.28
5	1.02	0.98	1.32	1.28
5.5	0.93	0.89	1.23	1.19
6	0.92	0.88	1.22	1.18
6.5	0.92	0.88	1.13	1.09
7	0.92	0.88	1.10	1.08
8	0.88	0.84	1.04	1.00
9	0.83	0.79	1.03	0.99

Since the coefficients V_{L}, V_{H}, C_{L} and C_{H} have been determined, the critical diameter d_{c} is only related to the remaining coefficients, namely,

$$d_{\mathrm{c}} = d_{\mathrm{c}}\left(V, \theta, S_{\mathrm{L}}, S_{\mathrm{H}}, X, X_{\mathrm{H}}\right) \tag{15}$$

These coefficients are obtained as $S_{\mathrm{L}} = 0.12$, $S_{\mathrm{H}} = 0.1$, $X = 0.48$ and $X_{\mathrm{H}} = 0.23$ by minimizing the mean square fitting error

$$e\left(S_{\mathrm{L}}, S_{\mathrm{H}}, X, X_{\mathrm{H}}\right) = \frac{1}{N}\sum_{k=1}^{N}(d_{\mathrm{c}}(V_k, \theta_k, S_{\mathrm{H}}, S_{\mathrm{L}}, X, X_{\mathrm{H}}) - \hat{d}_{ck})^2 \tag{16}$$

where $N = 44$ is the total number of points used to fit the equation, $d_{\mathrm{c}}\left(V_k, \theta_k, S_{\mathrm{L}}, S_{\mathrm{H}}, X, X_{\mathrm{H}}\right)$ is the fitted value and $\hat{d}_{ck}$ is the numerical value listed in Table 7.

Eventually, the eight determined coefficients of the ballistic limit equation for the multi-layer fabric coated aluminum plate are summarized in Table 8. The ballistic limit curves for impact angle $\theta = 0°$, $\theta = 45°$ and $\theta = 60°$ are plotted in Fig.21.

Table 8 Coefficients of the BLE for the multi-layer fabric coated aluminum plate

V_L	V_H	C_L	C_H	S_L	S_H	X	X_H
4.73	6.56	13	18	0.12	0.1	0.48	0.23

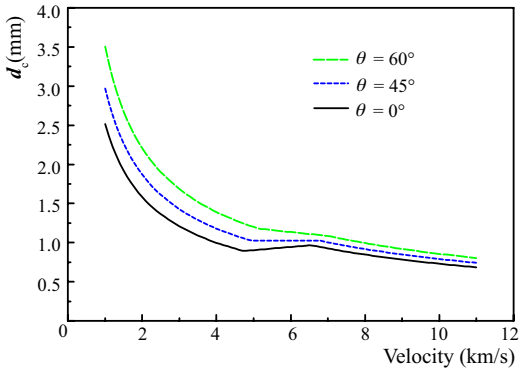

Fig. 21 Ballistic limit curves for impact angle $\theta = 0°$, $\theta = 45°$ and $\theta = 60°$

7 Conclusions

The ballistic limit equation plays an important role in determining the minimum shielding requirements for spacecraft. However, developing a ballistic limit equation based on hyper velocity tests is not only cost and time expensive, but also lacking of sufficient data for impact velocity higher than 7km/s due to the limitations of the experiment equipment capacity. Therefore, a validated numerical model is desirable to predict the hyper velocity impact behavior of spacecraft.

This study established a validated MPM model for the multi-layer fabric coated aluminum plate based on two hyper velocity tests. Numerical studies show that the validated MPM model can well predict the hyper velocity impact behavior of the multi-layer fabric coated aluminum plate with other impact velocities and projectile diameters. Hence, the validated MPM model can be used to provide hyper velocity impact data for impact velocity higher than 7km/s.

A ballistic limit equation is established for the multi-layer fabric coated aluminum plate for space suit design by using the hyper velocity test results for impact velocity less than 6.2km/s and the MPM simulation results for impact velocity greater than 6.2km/s. It shows that the critical diameter obtained by the validated MPM model for impact velocity less than 6.2km agrees well to the established ballistic limit equation, although which is established based on the test results for these velocity range.

The validated MPM model and the ballistic limit equation developed for the multi-layer fabric coated aluminum plate in this study provide an effective tool for the space suit design.

Acknowledgements This work was supported by the National Natural Science Foundation of China (Grant No. 11672154) and Science Challenge Project (TZ2017002).

References

1. Bintao L (2011) Research and application for special material models of spacecraft shielding structure. PhD thesis
2. Bohannan A, Fahrenthold E (2008) Hypervelocity impact simulation using membrane particle-elements. International Journal of Impact Engineering 35(12):1497–1502
3. Chen ZP, Qiu XM, Zhang X, Lian YP (2015) Improved coupling of finite element method with material point method based on a particle-to-surface contact algorithm. Computer Methods in Applied Mechanics and Engineering 293(15):1–19
4. Christiansen EL, Crews JL, Kerr JH, Chhabildas LC (1996) Hypervelocity impact testing above 10 km/s of advanced orbital debris shields. In: AIP Conference Proceedings, vol 370, pp 1183–1186
5. Christiansen EL, Cour-Palais BG, Friesen LJ (1999) Extravehicular activity suit penetration resistance. International Journal of Impact Engineering 23(1):113–124
6. Gleghorn G, Asay J, Atkinson D, Flury W, Johnson N, Kessler D, Knowles S, Rex D, Toda S, Veniaminov S (1969) Orbital debris: A technical assessment. Nasa Sti/recon Technical Report N 95
7. Gong WW, Liu Y, Zhang X, Ma HL (2012) Numerical investigation on dynamical response of aluminum foam subject to hypervelocity impact with material point method. CMES: Computer Modeling in Engineering & Sciences 83(5):527–545
8. Hayhurst C, Livingstone I (1998) Advanced Numerical Simulations for Hypervelocity Impacts: AUTODYN Simulation Final Report. Century Dynamics

9. Hosur MV, Vaidya UK, Ulven C, Jeelani S (2004) Performance of stitched/unstitched woven carbon/epoxy composites under high velocity impact loading. Composite Structures 64(3):455–466
10. Hua C (2013) Research on the mechanical and chemical properties of polyimide and its influence on hypervelocity impact phenomena. PhD thesis
11. Huang P, Zhang X, Ma S (2008) Shared memory OpenMP parallelization of explicit mpm and its application to hypervelocity impact. CMES-Computer Modeling in Engineering & Sciences 38:119–147
12. Huang P, Zhang X, Ma S, Huang X (2011) Contact algorithms for the material point method in impact and penetration simulation. International Journal for Numerical Methods in Engineering 85(4):498–517
13. Johnson GR, Cook WH (1983) A constitutive model and data for metals subjected to large strains, high strain rates, and high temperatures. In: Proc. of the 7th Intern. Symp. on Ballistics, pp 541–547
14. Johnson GR, Holmquist TJ (1988) Evaluation of cylinder-impact test data for constitutive model constants. Journal of Applied Physics 64(8):3901–3910
15. Lian Y, Yang P, Zhang X, Zhang F, Liu Y, Huang P (2015) A mesh-grading material point method and its parallelization for problems with localized extreme deformation. Computer Methods in Applied Mechanics and Engineering 289:291–315
16. Lian YP, Zhang X, Zhou X, Ma S, Zhao YL (2011) Numerical simulation of explosively driven metal by material point method. International Journal of Impact Engineering 38:237–245
17. Lian YP, Zhang X, Zhou X, Ma ZT (2011) A FEMP method and its application in modeling dynamic response of reinforced concrete subjected to impact loading. Computer Methods in Applied Mechanics and Engineering 200(17-20):1659–1670
18. Lian YP, Zhang X, Liu Y (2012) An adaptive finite element material point method and its application in extreme deformation problems. Computer Methods in Applied Mechanics and Engineering 241-244(1):275–285
19. Lian YP, Liu Y, Zhang X (2014) Coupling of membrane element with material point method for fluid–membrane interaction problems. International Journal of Mechanics and Materials in Design 10(2):199–211
20. Lian YP, Zhang X, Zhang F, Cui XX (2014) Tied interface grid material point method for problems with localized extreme deformation. International Journal of Impact Engineering 70:50–61
21. Liu P, Liu Y, Zhang X (2015) Improved shielding structure with double honeycomb cores for hypervelocity impact. Mechanics Research Communications 69:34–39
22. Liu P, Liu Y, Zhang X (2015) Internal-structure-model based simulation research of shielding properties of honeycomb sandwich panel subjected to high-velocity impact. International Journal of Impact Engineering 77:120–133
23. Liu P, Liu Y, Zhang X (2016) Simulation of hyper-velocity impact on double honeycomb sandwich panel and its staggered improvement with internal-structure model. International Journal of Mechanics and Materials in Design 12(2):241–254
24. Liu S, Huang J, Li Y, Zhou Z, Ma Z, Lan S, Chen H, Chen P (2011) Recent advancement of hypervelocity impact tests at hai, cardc. Manned Spaceflight (6):17–23
25. Liu Y, Wang HK, Zhang X (2013) A multiscale framework for high-velocity impact process with combined material point method and molecular dynamics. International Journal of Mechanics and Materials in Design 9(2):127–139
26. Ma S, Zhang X, Lian YP, Zhou X (2009) Simulation of high explosive explosion using adaptive material point method. CMES-Computer Modeling in Engineering & Sciences 39(2):101–123
27. Ma S, Zhang X, Qiu XM (2009) Comparison study of mpm and sph in modeling hypervelocity impact problems. International Journal of Impact Engineering 36(2):272–282
28. Ma Z, Zhang X, Huang P (2010) An object-oriented MPM framework for simulation of large deformation and contact of numerous grains. CMES-Computer Modeling in Engineering & Sciences 55(1):61–87
29. Mcallum WE (1969) Development of meteoroid protection for extravehicular-activity space suits. Journal of Spacecraft & Rockets 6(11)
30. Sulsky D, Chen Z, Schreyer HL (1994) A particle method for history-dependent materials. Computer Methods in Applied Mechanics and Engineering 118(1-2):179–196
31. Sulsky D, Zhou SJ, Schreyer HL (1995) Application of a particle-in-cell method to solid mechanics. Computer Physics Communications 87(1-2):236–252
32. White DM, Wicklein M, Clegg RA, Nahme H (2008) Multi-layer insulation material models suitable for hypervelocity impact simulations. International Journal of Impact Engineering 35(12):1853–1860
33. Zhang F, Zhang X, Liu Y (in press) An augmented incompressible material point method for modeling liquid sloshing problems. International Journal of Mechanics and Materials in Design DOI: 10.1007/s10999-017-9366-5
34. Zhang J (2004) Research of the mc nylon composite material stuffed with pulverized fuel ash. PhD thesis, Nanjing University of Science and Technology
35. Zhang X, Sze KY, Ma S (2006) An explicit material point finite element method for hyper velocity impact. International Journal for Numerical Methods in Engineering 66:689–706

36. Zhang X, Chen Z, Liu Y (2016) The Material Point Method - A Continuum-Based Particle Method for Extreme Loading Cases. Academic Press
37. Zukas JA (2004) Introduction to Hydrocodes. Elsevier Science